JOURNAL OF CATALYSIS 88, 188–202 (1984)

Deactivation Phenomena by Site Poisoning and Pore Blockage: The Effect of Catalyst Size, Pore Size, and Pore Size Distribution

K. S. TSAKALIS, T. T. TSOTSIS, AND G. J. STIEGEL*

*Department of Chemical Engineering, University of Southern California, Los Angeles, California 90089-1211 and *Pittsburgh Energy Technology Center, U.S. Department of Energy, Pittsburgh, Pennsylvania 15236*

Received September 27, 1983; revised February 17, 1984

The problem of catalyst deactivation by active site poisoning and pore blockage is analyzed. The effect of catalyst size, average pore size, and pore size distribution on the phenomenon of deactivation is investigated for two simple pore structure models, i.e., the "single pore" and "parallel bundle of pores" models. It is shown that the overall catalytic behavior and performance strongly depend on the catalyst's physical properties, such as its size, pore size, and pore size distribution. The mathematical models studied here are admittedly only oversimplified analogs of the complex physicochemical phenomena occurring during realistic industrial processes. The main qualitative features, however, of the overall catalytic behavior predicted here are the result of basic and strongly counteracting, underlying physicochemical processes. As such, the types of catalytic behavior described are not strongly dependent on the particular kinetic and diffusion models employed but are closely associated with macromolecular catalytic reaction systems that deactivate by simultaneous active site coverage and pore blockage.

INTRODUCTION

The phenomenon of catalyst deactivation has been the subject of intensive research activity in the fields of chemical reaction engineering and catalysis for the last 40 years. Since the pioneering work of Maxted (*1*), Voorhies (*2*), and Wheeler (*3*), a large number of papers have appeared dealing with different aspects of the phenomenon, among them several review papers (*4–9*).

Catalyst deactivation is a problem of particular severity for catalytic coal liquefaction and the hydrotreatment of coal-derived liquids. The cost of catalyst replacement resulting from catalyst deactivation could conservatively be placed in the range of $2 to $3 per bbl of oil processed. However, this is not necessarily the real problem, since the availability of catalytically active metals such as Co, Mo, and Ni is a more severe problem than their cost.

Over the last few years, considerable attention has been devoted to different experimental aspects of the phenomenon of deactivation occurring during catalytic coal liquefaction and catalytic hydrotreatment of coal-derived liquids. The experimental results have been presented in a series of recent publications and reports (*10–12*); a summary of the findings is presented here

(I) Severe activity losses, due to catalytic deactivation, occurred for the process times utilized, sometimes on the order of 50 to 60%.

(II) The losses in catalytic activity are accompanied by severe reductions (i.e., 50–60%) in both catalyst pore volume and surface area.

(III) Several modes of deactivation occur simultaneously, such as coke and metal deposition, irreversible adsorption of poisons (N-containing compounds), and sintering. It is very difficult to experimentally quantify the individual effect of each of these separate deactivation mechanisms. Evidence, however, does exist that for catalytic coal liquefaction in particular, deactivation occurs mainly by deposition of carbonaceous and, to a lesser extent, metal deposits, which deactivate the catalyst by

0021-9517/84 $3.00

simultaneous coverage of catalyst active sites and blockage of catalyst pores.

(IV) It has been shown experimentally (*10, 11*) that catalyst diameter, average pore size, and pore size distribution have a pronounced effect on overall catalyst performance.

In a recent publication (*10*), an effort was made to explain the effect of catalyst size on catalytic performance by use of simplified shell-type deactivation models. In this paper, a more extensive analysis of these phenomena is presented. A mathematical model that has been used with considerable success (*13, 14*) in modeling the experimental behavior of catalytic coal hydroliquefaction and coal-liquid hydrotreatment processes is studied in detail. The purpose of this study is to investigate theoretically the effect of catalyst size, average pore size, and pore size distribution on catalyst performance and to develop, when possible, simple algebraic expressions that predict a catalyst size, average pore size, and pore size distribution that yield the best overall catalyst performance and activity. Although the objective of this work was to obtain a better understanding of the deactivation phenomena occurring during catalytic coal liquefaction and the hydroprocessing of coal liquids, the results of this study could conceivably be applied to other industrial processes described by lumped kinetic models for which deactivation occurs by simultaneous site coverage and pore blockage.

THE MODEL

The first task in the study of coal hydroliquefaction or hydrotreatment processes is the selection of a proper kinetic model. During catalytic coal liquefaction in particular, a large number of reactions, such as HDN, HDS, hydrocracking, and hydrogenation, are known to occur simultaneously. Several mechanistic schemes have so far been proposed (*15*); unfortunately, the general validity of any of these mechanisms has yet to be completely proven.

It is well known however that if one is interested only in some particular aspect of the overall behavior of a complex reaction system, an accurate knowledge of the mechanistic picture is often not needed. Recently, Wei and Wei (*16*), Chang *et al.* (*14*), and Chiou and Olson (*13*) have successfully modeled deactivation phenomena occurring in hydroliquefaction and hydrotreatment processes using very simple lumped kinetic models. For catalytic coal hydroliquefaction, in particular for the simple parallel-type deactivation, a lumped kinetic model such as the one shown below has been suggested (*13, 14*).

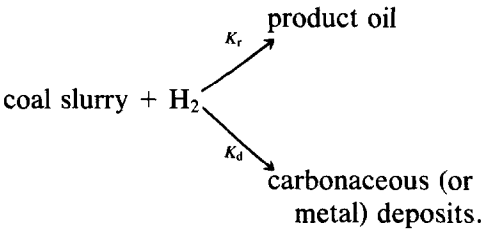

Here, "coal slurry" is taken to mean not only the feed coal slurry but also a whole class (or classes) of precursor molecules, such as preasphaltenes and asphaltenes, that result from coal by thermal degradation or direct solvent interaction. Hydrogen is usually present in excess, and the above lumped kinetic model is usually cast in the form

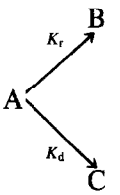

A, coal slurry; B, product oil; C, carbonaceous (or metal) deposits.

Progress in the quantitative analysis of the phenomenon of deactivation by site poisoning and pore blockage is strongly reliant upon the description of both the pore structure and the geometry of the foulant deposits. An adequate description of the complexities of the catalyst pore structure is still an issue to be settled. Although some

recent studies (*17–20*) have used stochastic pore models in an effort to understand the qualitative features of the phenomenon, the best currently available pore structure models that allow at least a semiquantitative insight are the single-pore and the so-called parallel bundle of pores models (*21*). The first pore structure model will be used in the investigation of the effect of particle size and average pore size, and the second in the analysis of the effect of pore size distribution.

THE SINGLE PORE MODEL

The catalyst pore structure will be assumed to be described by a set of N parallel straight pores of average radius r and half-length L; r, L, and N can be evaluated by means of measurable physical properties, such as porosity (ε), surface area (S_g, m^2/g), pore volume (V_g, cm^3/g), catalyst geometric volume (V_p, cm^3), and area (S_x, cm^2), and particle (ρ_p) and solid (ρ_s) densities (*3*). In the following discussion, the parallel-type deactivation problem previously described is considered. Furthermore, it will be assumed that deactivation occurs by a single type of deposits, and in accordance with experimental evidence from catalytic coal liquefaction and hydroprocessing of coal liquids (*11*), these deposits will be assumed to be of carbonaceous nature (i.e., coke). One could, of course, consider deactivation to occur by two or more types of deposits, such as metals and irreversibly adsorbed compounds. This, however, is not needed here, since the problem then becomes hopelessly complex, while evidence exists that the main conclusions and results of this study remain basically unchanged (*22*). In accordance with experimental observations (*11, 23*), both the main and the fouling reactions will be assumed to follow pseudo-first-order, single-site kinetics. The corresponding species conservation balances for a single pore are

$$\frac{\partial(\varepsilon_p C_A)}{\partial t} = \frac{\partial}{\partial x}\left(D_{Ae}\frac{\partial C_A}{\partial x}\right) - \frac{2}{r}K_r[1 + Sa]C_A(C_t - C_{cs}) \quad (1)$$

$$\frac{\partial(\varepsilon_p C_B)}{\partial t} = \frac{\partial}{\partial x}\left(D_{Be}\frac{\partial C_B}{\partial x}\right) + \frac{2}{r}K_r C_A(C_t - C_{cs}) \quad (2)$$

$$\frac{\partial C_{cs}}{\partial t} = K_d C_A(C_t - C_{cs}) \quad (3)$$

with boundary conditions

$$x = 0; \qquad \frac{\partial C_A}{\partial x} = \frac{\partial C_B}{\partial x} = 0 \quad (4a)$$

$$x = L; \qquad C_A = C_{A0},\ C_B = 0 \quad (4b)$$

and initial conditions

$$t = 0; \qquad C_{cs} = 0 \quad (5a)$$

$$\frac{\partial}{\partial x}\left(D_{Ae}\frac{\partial C_A}{\partial x}\right) - \frac{2}{r}K_r C_A C_t = 0 \quad (5b)$$

$$\frac{\partial}{\partial x}\left(D_{Be}\frac{\partial C_B}{\partial x}\right) + \frac{2}{r}K_r C_A C_t = 0. \quad (5c)$$

For the porosity and effective diffusivities, use will be made of semiempirical relationships successfully utilized in prior investigations

$$\varepsilon_p = 1 - b\left(\frac{C_{cs}}{C_t}\right) \quad (6a)$$

$$b = \frac{V_c C_t \pi_0}{A_0}, \quad (6b)$$

and

$$D_{ie} = D_{i0}\varepsilon_p F(\lambda_i),\ \lambda_i = \lambda_{i0}\varepsilon_p^{-1/2}, \quad (7a)$$

$$\lambda_{i0} = \left(\frac{A_{im}}{A_0}\right)^{1/2} = \left(\frac{r_{im}}{r}\right), \quad (7b)$$

where

$$F(\lambda_i) = 0 \qquad \text{when } \lambda_i \geq 1 \quad (7c)$$

$$F(\lambda_i) = \exp(-4.6\,\lambda_i) \qquad \text{when } \lambda_i < 1. \quad (7d)$$

Equation (7) is a semiempirical relation-

ship developed by Satterfield *et al.* (*24, 25*) that is used to describe diffusion of macromolecules with "effective" diffusion diameters of the same order of magnitude as the catalyst pores, typical of the macromolecules involved in catalytic coal liquefaction. Equations (1)–(5) can be made dimensionless as (The different dimensionless symbols are defined in the nomenclature section.)

$$\gamma_1 \frac{\partial}{\partial \theta}(\varepsilon_p X) = \frac{\partial}{\partial \xi}\left[\varepsilon_p F(\lambda_A)\frac{\partial X}{\partial \xi}\right] - \phi^2 \lambda_{A0} X[1 + Sa](1 - Z) \quad (8)$$

$$\gamma_1 \frac{\partial}{\partial \theta}(\varepsilon_p Y) = \gamma_2 \frac{\partial}{\partial \xi}\left[\varepsilon_p F(\lambda_B)\frac{\partial Y}{\partial \xi}\right] + \phi^2 \lambda_{A0} X[1 - Z] \quad (9)$$

$$\frac{\partial Z}{\partial \theta} = X(1 - Z) \quad (10)$$

and

$$\varepsilon_p = 1 - b_1 \lambda_{A0} Z$$

with boundary conditions

$$\xi = 0; \qquad \frac{\partial X}{\partial \xi} = \frac{\partial Y}{\partial \xi} = 0 \quad (11a)$$

$$\xi = 1; \qquad X = 1,\ Y = 0 \quad (11b)$$

and initial conditions

$$\theta = 0; \qquad Z = 0 \quad (12a)$$

$$\frac{\partial^2 X}{\partial \xi^2} = \phi^2 \left(\frac{\lambda_{A0}}{F(\lambda_{A0})}\right) X \quad (12b)$$

$$\gamma_2 \frac{\partial^2 Y}{\partial \xi^2} = -\phi^2 \left(\frac{\lambda_{A0}}{F(\lambda_{B0})}\right) X \quad (12c)$$

The rates of reaction for the particle are given as

$$-R_A^P = V_p \rho_p S_g K_r C_t C_{A0} \eta_A(\theta) \quad (13a)$$

$$R_B^P = V_p \rho_p S_g K_r C_t C_{A0} \eta_B(\theta), \quad (13b)$$

where

$$\eta_A(\theta) = \frac{\varepsilon_p F(\lambda_A)\left.\frac{\partial X}{\partial \xi}\right|_{\xi=1}}{\lambda_{A0}\phi^2} \quad (14a)$$

$$\eta_B(\theta) = \frac{-\gamma_2 \varepsilon_p F(\lambda_B)\left.\frac{\partial Y}{\partial \xi}\right|_{\xi=1}}{\lambda_{A0}\phi^2}. \quad (14b)$$

I. Optimal Initial Activity

When catalytic deactivation is absent or unimportant, one usually optimizes reactor design by selecting the catalyst with maximum initial activity. When the catalytic system under study is rapidly deactivating, as is the case with catalytic coal liquefaction, the catalyst with the maximum initial activity often does not exhibit (as it was first shown by Rajagopalan and Luss (*26*)) an overall optimum performance. Even under these circumstances one needs to know the maximum initial activity value, since this value is the obvious choice as a basis in activity optimization studies.

In studies of reactor design and optimization, one usually compares existing catalysts in terms of either activity per unit volume or activity per unit weight. Activities per unit volume or per unit weight can be calculated of course by Eq. (13) by dividing V_p or $V_p\rho_p$.

Furthermore for the single pore model, one can manipulate the size of the average catalyst pore radius by changing either V_g or S_g or both. Two different cases will be investigated in this paper. In the first case, changes in V_g will be allowed for, but S_g will be kept constant, while in the second case, V_g will be kept constant, and S_g will be allowed to vary.

When V_g stays constant, ε and ρ_p also stay constant. Since activity per unit volume (R_A^V) is related to the activity per unit weight (R_A^W) as $R_A^V = R_A^W/\rho_p$ for this case R_A^V and R_A^W follow the same type of behavior in terms of λ_{A0} (or r for constant r_{Am}); R_A^V is given by the relationship

$$-R_A^V = \left(\frac{2\varepsilon}{r_{Am}} K_r C_t C_{A0}\right) \lambda_{A0}\eta_A = P_1 \lambda_{A0}\eta_A. \quad (15)$$

If one assumes that K_r, C_t (which depend on the catalyst's chemical composition),

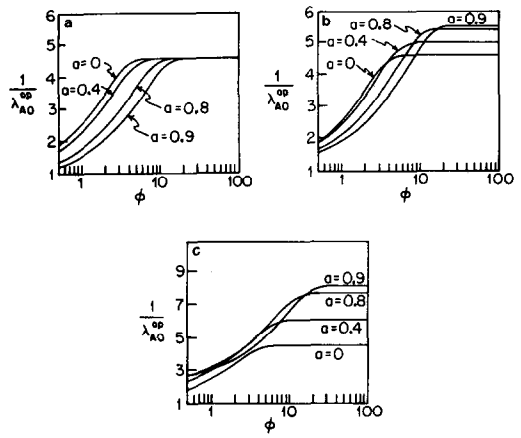

FIG. 1. Plot of $1/\lambda_{A0}^{op}$ versus ϕ for the case of uniform fouling and a constant value of V_g. (a) $b_1 = 0$. (b) $b_1 = 0.5$. (c) $b_1 = 2$.

and r_{Am} (which depends on the size of the reactant molecule) remain constant, P_1 is a constant.

A value of $\lambda_{A0}(\lambda_{A0}^{iop})$ that maximizes $(-R_A^V)$ at $\theta = 0$ (initial activity) can be found implicitly in terms of the equation (*26*)

$$[1 + 4.6\lambda_{A0}]\left[1 - \frac{2\phi_I}{\sinh 2\phi_I}\right] = 2, \quad (16a)$$

where

$$\phi_I = \phi\left(\frac{\lambda_{A0}}{F(\lambda_{A0})}\right)^{1/2}. \quad (16b)$$

$(1/\lambda_{A0}^{iop})$ is plotted as a function of ϕ in Fig. 1. (The curve corresponding to $\alpha = 0$.) Note that as ϕ increases, $1/\lambda_{A0}^{iop}$ increases (r^{iop} decreases for r_{Am} constant), and for $\phi \to \infty$, $1/\lambda_{A0}^{iop} \to 4.6$.

When S_g stays constant, R_A^V and R_A^W are given by the relationships

$$-R_A^V = \frac{S_g\rho_s K_r C_t C_{A0}\lambda_{A0}}{\frac{\rho_s S_g r_{Am}}{2} + \lambda_{A0}}\eta_A$$

$$= \frac{P_2\lambda_{A0}}{P_3 + \lambda_{A0}}\eta_A \quad (17a)$$

$$-R_A^W = S_g K_r C_t C_{A0}\lambda_{A0}\eta_A = P_4\eta_A. \quad (17b)$$

There is no λ_{A0} for this case that maximizes $(-R_A^W)$ at $\theta = 0$. However, a value of λ_{A0} does exist that maximizes $(-R_A^V)$ at $\theta = 0$, which is given by the relationship

$$[1 + 4.6\lambda_{A0}][P_3 + \lambda_{A0}]\left[1 - \frac{2\phi_I}{\sinh 2\phi_I}\right] = 2P_3. \quad (18)$$

(For a typical hydroprocessing catalyst (*11, 12*), $P_3 \simeq 0.5$.) When $(1/\lambda_{A0}^{iop})$ for this case, is plotted as a function of ϕ the behavior is quite similar with that shown in Fig. 1 for the previous case.

II. Some Simple Models Based on the Quasi-Steady-State Hypothesis

It has been customary through the years in the field of catalyst deactivation particularly for catalytic reactor design problems, to work with simplified models based on the quasi-steady-state hypothesis. Such models for simple poisoning have been analyzed by Masamune and Smith (*27*). In this study, similar models will be analyzed for the case of deactivation by site coverage and pore plugging. Two types of deactivation will be dealt with, namely, uniform-type deactivation and shell-type deactivation.

(*A*) *Uniform deactivation.* For this type of deactivation, the assumption made is that the deactivation process is slow, so that coke deposition occurs uniformly throughout the pore. If α is the fraction of sites covered by coke, then the rate per catalyst particle is given as

$$-R_A^P = R_B^P = V_p\rho_p S_g K_r C_t C_{A0}(1 - \alpha)\eta, \quad (19a)$$

where

$$\eta = \frac{\tanh\phi_u}{\phi_u}, \quad (19b)$$

$$\phi_u = \phi\left[\frac{\lambda_{A0}(1 - \alpha)}{F(\lambda_A)\varepsilon_p}\right]^{1/2}. \quad (19c)$$

Note that for

$$\alpha \geq \frac{1 - \lambda_{A0}^2}{b_1\lambda_{A0}} \quad (b_1, \lambda_{A0} \neq 0) \quad (19d)$$

the pores are plugged and the catalyst is completely deactivated. The goal here is to examine the system behavior in terms of ϕ

(i.e., catalyst diameter) and $(1/\lambda_{A0})$ (i.e., r/r_{Am}) for different values of α.

Since V_g or S_g do not depend on ϕ (and therefore L), whatever the value of α, there is no L that maximizes either activity per unit weight or per unit volume. As α changes, the activities of catalysts with different ϕ do approach each other, and for $\alpha \to ((1 - \lambda_{A0}^2)/b_1\lambda_{A0})$ the activities vanish; however, the catalysts retain the same ordering in activities that they had at $\alpha = 0$ up to complete deactivation.

The effect of r (or $1/\lambda_{A0}$) is, however, quite interesting. If one keeps V_g constant and allows S_g to change, a value of λ_{A0} (defined as λ_{A0}^{op}) exists that maximizes $(-R_A^V)$ and $(-R_A^W)$, which is the solution of the equation

$$\left(1 - \frac{2\phi_u}{\sinh 2\phi_u}\right)[1 + 2.3(2 - b_1\lambda_{A0}\alpha)(1 - b_1\lambda_{A0}\alpha)^{-1/2}\lambda_{A0}] = 2(1 - b_1\lambda_{A0}\alpha). \quad (20)$$

For this case, λ_{A0}^{op} is a function of both b_1 and α. In Fig. 1a, $1/\lambda_{A0}^{op}$ is plotted as a function of ϕ, with parameter α for $b_1 = 0$ (simple poisoning). Note that as α increases (for constant ϕ), $(1/\lambda_{A0}^{op})$ (and therefore r^{op}) decreases. However, for large ϕ, all curves tend to the same asymptotic value. To understand the behavior shown on Fig. 1a, one should look at Fig. 2a, where $(-R_A^V/P_1)$ is plotted as a function of λ_{A0} with parameter α. As α increases $(-R_A^V/P_1)$ decreases and, simultaneously, the maximum in the rate moves toward a larger value of λ_{A0}^{op} (smaller values of r^{op}). The curve corresponding to $\alpha = 0$ is the initial optimum activity curve. From Fig. 2a, one should expect the following behavior for two catalysts with otherwise similar properties but different λ_{A0} values. If both catalysts have r smaller than r^{iop} (the r value corresponding to λ_{A0}^{iop}), then initially the catalyst with the larger r (smaller λ_{A0} value) will have higher activity. However, as time increases (α increases), the activity of the catalyst with the smaller r (higher λ_{A0} value) will become

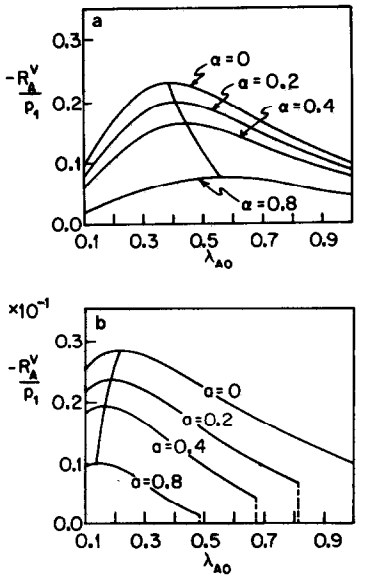

FIG. 2. Plot of $(-R_A^V/P_1)$ versus λ_{A0} for the case of uniform fouling and a constant value of V_g. (a) $b_1 = 0$; $\phi = 1$. (b) $b_1 = 2$; $\phi = 10$.

larger than the activity of the catalyst with the larger r (smaller λ_{A0} value), i.e., the phenomenon of catalytic activity crossover will occur. If the two catalysts, on the other hand, have r values larger than the optimum r^{iop} value, then the catalyst with the smaller r will have higher initial activity and will remain more active than the catalyst with the larger r up to complete deactivation. The behavior described so far is shown in Fig. 3a, where we plot $(-R_A^V/P_1)$ as a function of α with parameter λ_{A0}. The type of behavior shown in Fig. 3a has also been observed experimentally during catalytic coal liquefaction and coal–liquid hydrotreatment processes (*11, 12*).

In Figs. 1b and c, $1/\lambda_{A0}^{op}$ is plotted as a function of ϕ for different values of α and two values of b_1 (= 0.5 and 2). Note that for large ϕ, the behavior of $1/\lambda_{A0}^{op}$ as a function of ϕ (for the region of α values shown in Figs. 1b and c) is quite opposite to the behavior shown in Fig. 1a. As α increases, $1/\lambda_{A0}^{op}$ moves toward higher values. In Fig. 2b, $(-R_A^V/P_1)$ is plotted versus λ_{A0} for this case. As α increases, the activity declines and the maximum moves toward lower values of

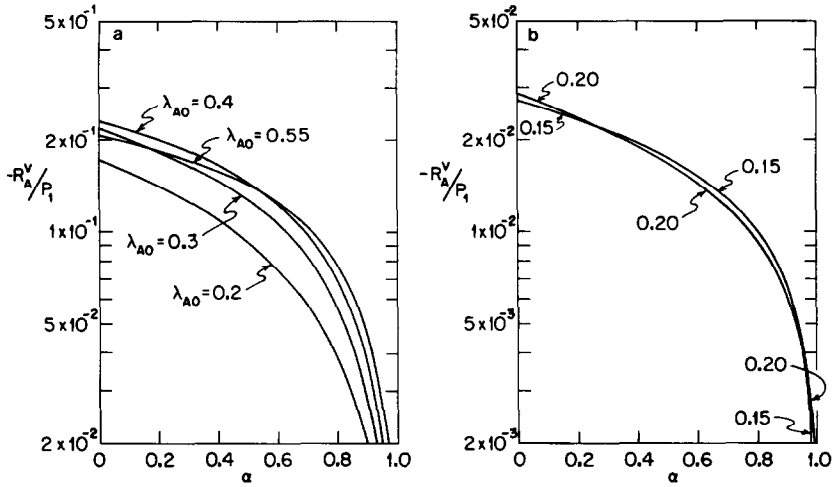

FIG. 3. Plot of $(-R_A^V/P_1)$ versus α for the case of uniform fouling and a constant value of V_g. (a) $b_1 = 0$; $\phi = 1$. (b) $b_1 = 2$; $\phi = 10$.

λ_{A0}. This, of course, means that a crossover in activities will now occur for two catalysts with r values larger than r^{op}, which is exactly opposite to what is expected for $b_1 = 0$. For intermediate ranges of ϕ values (or sufficiently large values of α), the behavior is quite complex, and as α increases, $1/\lambda_{A0}^{op}$ first increases (r^{op} decreases) and then decreases (r^{op} increases). For an appropriate set of b_1 ϕ, λ_{A0}, and α values, this could, of course, result in a double-crossover in activity, as shown in Fig. 3b.

For the case where S_g stays constant but V_g is allowed to change, one can once more verify that no value of λ_{A0} exists that maximizes $(-R_A^W)$ for any value of α. However, a value of λ_{A0} exists that maximizes $(-R_A^V)$, which is the solution of the equation

$$\left(1 - \frac{2\phi_u}{\sin 2\phi_u}\right)(P_3 + \lambda_{A0})$$
$$[1 + 2.3\lambda_{A0}(2 - b_1\lambda_{A0}\alpha)(1 - b_1\lambda_{A0}\alpha)^{-1/2}]$$
$$= 2P_3(1 - b_1\lambda_{A0}\alpha). \quad (21)$$

The behavior of λ_{A0}^{op} as a function of α, ϕ, and b_1 for this case is very similar to the behavior shown in Figs. 1 and 2.

In conclusion, it has to be pointed out that due to the large number of different feedstocks, catalysts and operating conditions used during catalytic coal liquefaction and coal-liquid hydrotreatment processes, and to the experimental uncertainty in the calculation of system parameters the ranges of typical values of ϕ, λ_{A0}, and b_1 are quite large. Typical values for ϕ lie between 0 and 20 and for λ_{A0} between 0.1 and 0.6.

(B) The shrinking core model. Shell or shrinking-core models have been used extensively in several areas of chemical engineering. For problems of simple poisoning, the model has been developed by Masamune and Smith (*27*). For the case of deactivation by site coverage and pore plugging, for the shell model to be valid

$$b_1 \leq \frac{(1 - \lambda_{A0}^2)}{\lambda_{A0}}. \quad (22)$$

If Eq. (22) is not satisfied, the outside deactivated shell will be plugged completely, and the catalyst will be rendered inactive immediately. If Eq. (22) is satisfied, then the effectiveness factor for the single pore is given as

$$\eta = \frac{B(1 - x_{Ai})}{(1 - \xi_i)} \Big/ \phi_1^2, \quad (23a)$$

where

$$x_{Ai} = \frac{B}{B + (1 - \xi_i)\phi_I \tanh(\phi_I \xi_i)}, \quad (23b)$$

$$\theta = \frac{\phi_I^2}{2B}[(\xi_i - 1)^2] - \ln\left[\frac{\sinh(\phi_I \xi_i)}{\sinh \phi_I}\right], \quad (23c)$$

$$B = \frac{(1 - b_1\lambda_{A0})F(\lambda_{A0}(1 - b_1\lambda_{A0})^{-1/2})}{F(\lambda_{A0})}. \quad (23d)$$

For the case of uniform fouling, it was shown that ϕ (i.e., the diameter of the particle) has no qualitatively interesting effect on the overall deactivation behavior, and no crossover in activity is observed from $\alpha = 0$ up to complete deactivation. For shell-type deactivation, however, as θ increases ($\theta \neq 0$), a value of $\phi(\phi_{op})$ that maximizes activity appears. This behavior is shown in Fig. 4, where ϕ_{op} is plotted as a function of θ, and in Fig. 5, where $(-R_A^V/P_1)$ is plotted versus ϕ, with time as a parameter.

Therefore, if one compares two catalysts that have otherwise similar properties but different diameters, initially the catalyst with the smaller diameter will have higher activity (both in terms of activity per unit volume and per unit weight). However, as deactivation proceeds, the activity of the catalyst with the larger diameter approaches the activity of the catalyst with the smaller diameter until at a given process time, there will be a crossover in activity. This type of behavior has also been observed experimentally for the coal hydroliquefaction process (*11*). As λ_{A0} (or b_1) increases, ϕ_{op} decreases (Fig. 4). Note that for $\theta = 0$, $\phi_{op} = 0$ as expected.

The effect of λ_{A0} on catalytic activity for this case is shown in Figs. 6 and 7. In Figs. 6a and b, $1/\lambda_{A0}^{op}$ (where λ_{A0}^{op} is the value of λ_{A0} that maximizes both $(-R_A^V)$ and $(-R_A^W)$) is plotted versus ϕ for the case for which V_g stays constant but S_g changes. In Figs. 6c and d, $1/\lambda_{A0}^{op}$ (where λ_{A0}^{op} is the value of λ_{A0} that maximizes $(-R_A^V)$) is plotted versus ϕ for the case where S_g stays constant but V_g

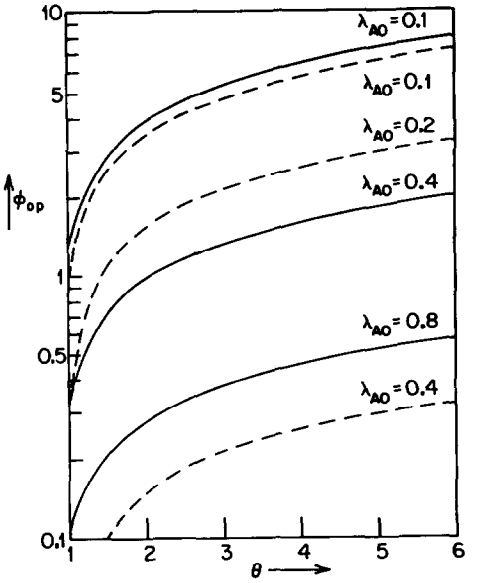

FIG. 4. Plot of ϕ_{op} versus time for the shell deactivation model. (——) $b_1 = 0$; (– – –) $b_1 = 2$.

changes. Note that Fig. 6 is qualitatively similar to Fig. 1.

The most interesting type of behavior is shown, however, in Fig. 7. For the case of shell deactivation, a value of λ_{A0} exists that maximizes $(-R_A^W)$. In Fig. 7, $1/\lambda_{A0}^{op}$ for this case is plotted as a function of ϕ. Note that $(1/\lambda_{A0}^{op})$ approaches infinity as θ approaches zero as expected (since it has already been shown that at $\theta = 0$, there is no λ_{A0} maxi-

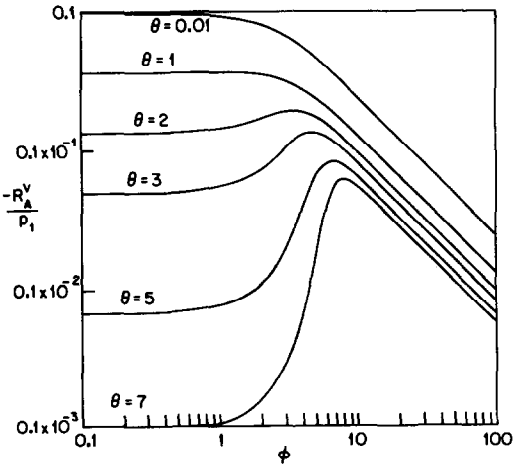

FIG. 5. Plot of $(-R_A^V/P_1)$ versus ϕ for the shell deactivation model. $b_1 = 2$; $\lambda_{A0} = 0.1$.

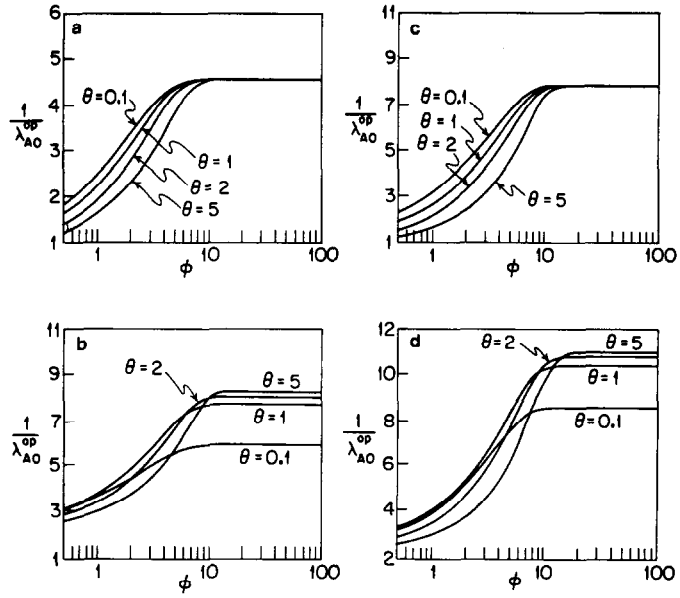

FIG. 6. Plot of $(1/\lambda_{A0}^{op})$ versus ϕ for the shell deactivation model and a constant value of V_g. (a) $b_1 = 0$; (b) $b_1 = 2$; for a constant value of S_g. (c) $b_1 = 0$; (d) $b_1 = 2$.

mizing $(-R_A^W)$). Note furthermore that as b_1 increases, $(1/\lambda_{A0}^{op})$ also increases.

III. The Complete Deactivation Model

The complete set of Eqs. (1)–(5) has been solved by a modified Crank-Nicolson implicit finite difference scheme. A detailed description of the numerical scheme used can be found elsewhere (*22*). In solving Eqs. (1)–(5), the following simplifying assumption has been used:

$$\gamma_2 = \frac{D_{B0}}{D_{A0}} \approx \frac{r_{Am}}{r_{Bm}}. \tag{24a}$$

Note furthermore that γ_1 is given as

$$\gamma_1 = \beta\phi^2 S; \tag{24b}$$

$$\beta = \left(\frac{C_{A0} r_{Am}}{C_t}\right). \tag{24c}$$

In the numerical solution of the problem, β is taken equal to 3×10^{-2}, a value typical of the reaction system and reaction conditions employed (*11, 12*).

A detailed quantitative account of all the features of the optimization problem for the completely distributed physical model described by Eqs. (1)–(5) is not presented but can be found elsewhere (*22*). Instead, typical results are presented in Figs. 8–10 used to show that the physical model described by the complete distributed set of Eqs. (1)–

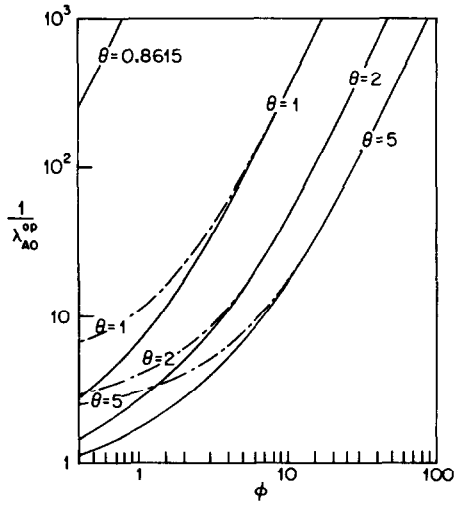

FIG. 7. Plot of $(1/\lambda_{A0}^{op})$ for $-R_A^W$ versus ϕ for the shell deactivation model and a constant value of S_g. (——) $b_1 = 0$. (–·–·) $b_1 = 2$.

(5) exhibits the same overall qualitative behavior as the simple shell-type deactivation model, which has been analyzed completely. In Fig. 8, (R_B^W/P_1) is plotted versus ϕ for $b_1 = 2$, $S = 0.08$, and $\gamma_2 = 2$. Note that the behavior shown in Fig. 8 is qualitatively similar to the behavior shown in Fig. 5, but as expected, differences do exist in both the values of the optimum ϕ and the levels of catalytic activity.

The same can be said when one compares the behavior shown in Figs. 9 and 10 with the behavior exhibited by the shell deactivation model and corresponding Figs. 6b, d, and 7.

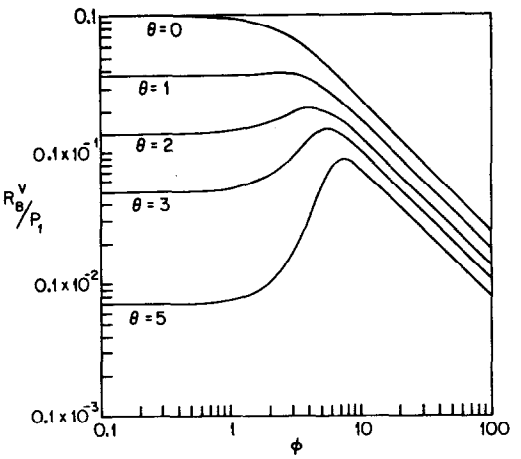

FIG. 8. Plot of (R_B^V/P_1) versus ϕ for the deactivation model described by Eqs. (1)–(5). $b_1 = 2$, $\lambda_{A0} = 0.1$, $S = 0.08$, $\gamma_2 = 2$, $\alpha = 1$.

THE EFFECT OF PORE SIZE DISTRIBUTION—THE PARALLEL BUNDLE OF PORES MODEL

The parallel bundle of pores model has found extensive and frequent use in several areas of chemical reaction engineering, since it is the simplest pore model that can account for realistic pore structures characterized by a pore size distribution. Beyond its simplicity, the parallel bundle of pores model is of particular importance, since it is the only model (on an almost universal basis) utilized in the interpretation and presentation of BET and mercury porosimetry data of commercially available catalysts.

According to this model (*21*), the catalyst particles consist of N straight cylindrical pores with an average half-length L and with radii that follow a pore size number probability distribution function $f_N(r)$ (i.e., $Nf_N(r)dr$ is the number of pores with a radius between r and $r + dr$) and a pore size volume probability function $f_V(r)$. In this study, the activity of catalysts having the same porosity (ε, ρ_p, V_g constant) but different pore size distributions will be compared. Since ρ_p is assumed constant, the activity comparison basis can be either rate per unit volume or rate per unit weight.

The surface area per unit volume, S_g, can then be expressed as

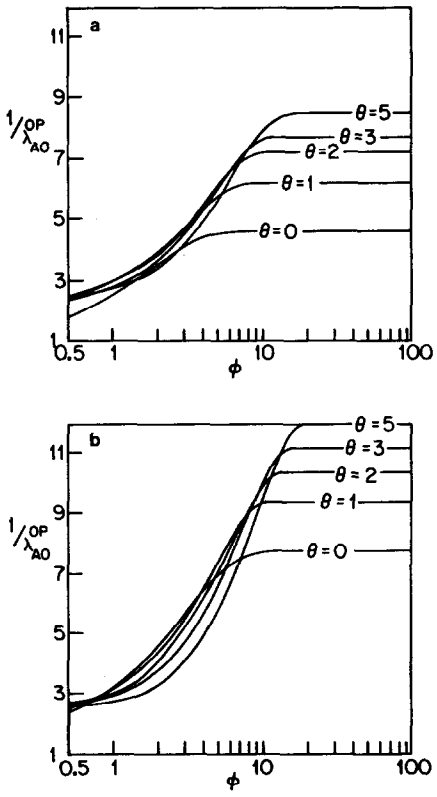

FIG. 9. Plot of $(1/\lambda_{A0}^{OP})$ versus ϕ for the deactivation model described by Eqs. (1)–(5). $b_1 = 2$, $S = 0.08$, $\gamma_2 = 2$, $\alpha = 1$. (a) For a constant value of V_g; (b) for a constant value of S_g.

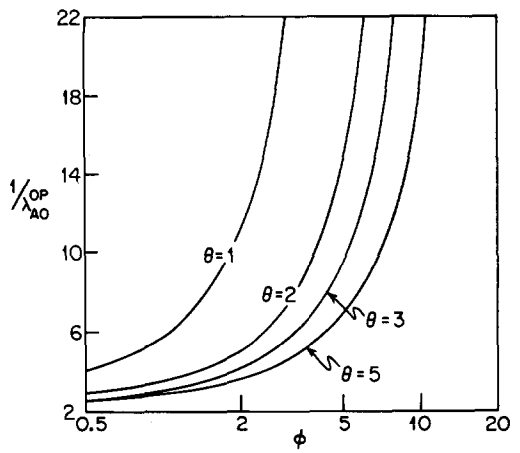

FIG. 10. Plot of $(1/\lambda_{A0}^{op})$ for $(-R_A^W)$ versus ϕ for the deactivation model described by Eqs. (1)–(5). S_g constant. $b_1 = 2$, $S = 0.08$, $\gamma_2 = 2$, $\alpha = 1$.

$$S_g = \frac{2\varepsilon}{\rho_p}\int_0^\infty \frac{f_V(r)dr}{r} \tag{25}$$

and the rate per unit volume can be expressed as

$$R_B^P = 2\varepsilon K_r C_t C_{A0}\int_0^\infty \frac{f_V(r)\eta_B(r,\theta)dr}{r}, \tag{26}$$

where $\eta_B(r,\theta)$ is given by Eq. (14).

Catalysts with unimodal pore size distributions will be considered here, and attention will be limited to log-normal-type pore size distributions, which adequately describe the pore size distribution of most unimodal liquefaction catalysts. Therefore, it will be assumed that $f_V(r)$ is described by the equation

$$f_V(r) = \frac{1}{r\sigma\sqrt{2\pi}}\exp\left[-\frac{[\ln(r/\hat{r})]^2}{2\sigma^2}\right]. \tag{27}$$

Furthermore, attention will be focused on deactivation phenomena described by Eqs. (1)–(5). There is a considerable amount of computational effort involved in the study of the behavior of a catalyst particle with a pore size distribution described by Eq. (27), for which each pore in the distribution is described by Eqs. (1)–(5). Detailed accounts of the numerical methods and analysis techniques used can be found elsewhere (*22*). The first goal here is to determine values (if any) of σ and $\hat{r}$ (or $\hat{\lambda}_{A0}$) that optimize initial catalytic activity ($\theta = 0$). In Fig. 11, the value of $\sigma(\sigma_{iop})$ that maximizes initial catalytic activity is plotted as a function of $\hat{\lambda}_{A0}$ (median λ_{A0} value) with parameter ϕ. There is a region of $\hat{\lambda}_{A0}$ values in Fig. 11 for which the corresponding σ_{iop} values are smaller than the accuracy limit of our numerical techniques (0.01). On either side of this region, σ_{iop} is positive and greater than 0.01.

It is easy to prove analytically that for $\hat{\lambda}_{A0} = \lambda_{A0}^{iop}$, $\sigma = 0$. This is not necessarily so, however, for values of $\hat{\lambda}_{A0} \neq \lambda_{A0}^{iop}$. It is of interest that (as shown in Fig. 11) regions of $\hat{\lambda}_{A0}$ values do exist for which $\sigma_{iop} \neq 0$. However, since the absolute maximum value in initial activity corresponds to $\hat{\lambda}_{A0} = \lambda_{A0}^{iop}$ for which $\sigma_{iop} = 0$ this could simply be only a matter of academic curiosity. The effect of deactivation on catalytic activity is shown in Fig. 12, where the value of $\sigma(\sigma_{op})$ of the catalyst with the maximum catalytic activity is plotted as a function of θ after the onset of the deactivation process. Note that the σ value plotted in Fig. 12 is the shape factor of the pore size distribution for the fresh catalyst and does not characterize in any direct way the pore size distribution of the deactivated catalyst at time θ. The behavior shown in Fig. 12 is complex and is rather sensitive to changes in the values of the parameters $\hat{\lambda}_{A0}$, b_1, and ϕ. This behavior is the result of the effects brought up by the phenomenon of pore blockage on the pore size distribution curve combined with the type of activity changes, due to deactivation, expected in each pore (Figs. 8–10).

For $\hat{\lambda}_{A0}$ equal to 0.3 or 0.4 in Fig. 12a, $\sigma_{iop} = 0$, and σ_{op} increases as time increases. This, of course, means that if one is to start with two fresh catalysts of otherwise similar properties but with pore size distributions characterized by different σ's, then the catalyst with the uniform pore size distribution ($\sigma = 0$) will initially have higher activity. However, at later times, the activity of the catalyst with the nonuniform pore size distribution will eventually exceed

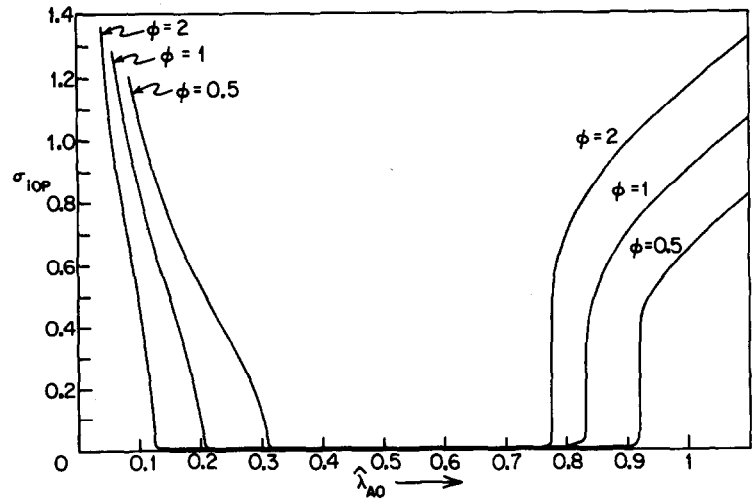

FIG. 11. Plot of σ_{iop} versus $\hat{\lambda}_{A0}$.

(crossover) the activity of the catalyst with the uniform pore size distribution.

If the value of $\hat{\lambda}_{A0}$ is such, however, the $\sigma_{iop} \neq 0$, then the phenomenon of activity crossover will only occur if one starts with two fresh catalysts with σ's larger than σ_{iop} (Fig. 13). The phenomenon of catalytic activity crossover will not occur for catalysts with σ smaller than σ_{iop}.

When $b_1 \neq 0$ the catalytic behavior predicted is very complex (see Fig. 12b). Two (for $\hat{\lambda}_{A0}$ equal to 0.1, 0.15, 0.17 in Fig. 12b), three (for $\hat{\lambda}_{A0}$ equal to 0.2 and 0.3), and four (not shown in Fig. 12b but occurring for $\hat{\lambda}_{A0}$ equal to 0.2 and 0.3 and for θ larger than 10) activity crossover points are theoretically feasible (22) for the log-normal-type pore size distribution function (Eq. (27)) and the deactivation behavior described by Eqs. (1)–(5). The case with three activity crossover points is shown in Fig. 13b, where R_B/P_1 is plotted as a function of time with σ as a parameter.

Cases with more than one activity crossover points have yet to be observed experimentally. In our theoretical calculations,

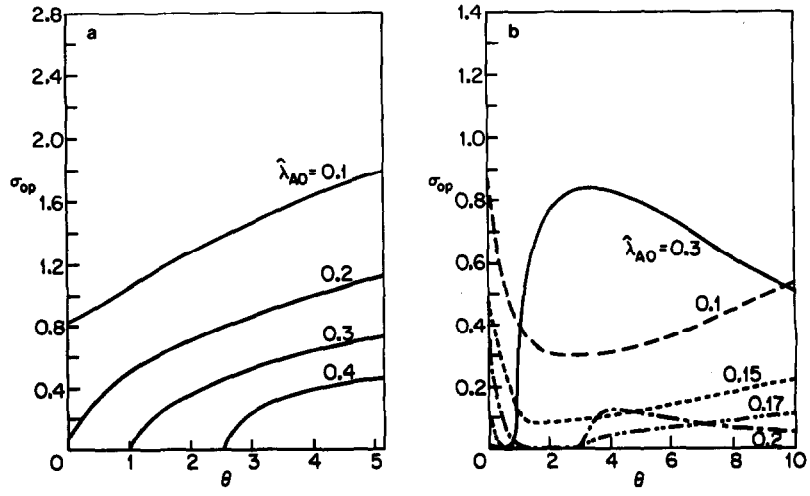

FIG. 12. Plot of σ_{op} versus θ, $S = 0.08$, $\phi = 1$, $\gamma_2 = 2$, $\alpha = 1$. (a) $b_1 = 0$; (b) $b_1 = 5$.

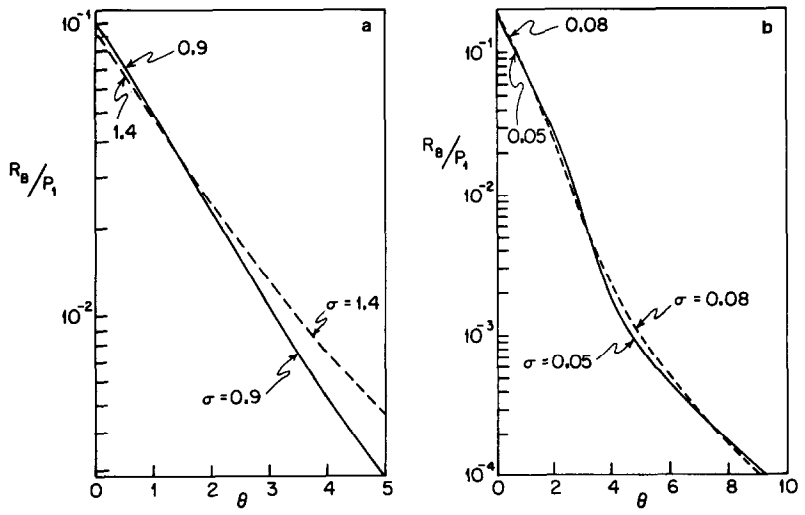

FIG. 13. Plot of (R_B/P_1) versus θ, $S = 0.08$, $\phi = 1$, $\gamma_2 = 2$, $\alpha = 1$. (a) $b_1 = 0$; $\lambda_{A0} = 0.1$. (b) $b_1 = 5$; $\lambda_{A0} = 0.2$.

the additional activity crossover points normally occur at large integration times, at which point the activity of both catalysts has considerably decreased. It is conceivable that, at this point, in real experimental situations the experimental uncertainty involved in the measurement of catalytic reaction rates far exceeds measurable differences in catalytic activity.

Finally it should be pointed out that in this study it has been assumed that the coke (or metal) deposits are totally inactive with respect to the main reaction and that their nature does not change throughout the whole process. It has recently become apparent, however, that during coal liquefaction and catalytic hydrotreatment of coal-derived liquids this is not necessarily true. These deposits appear to be initially active participants in the reaction and their activity and nature change slowly with process time (as indicated, for example, by a decline in the H/C ratio of the coke deposits). A theoretical investigation to account for such behavior is currently in progress.

CONCLUSIONS

In this study, the behavior of catalysts that are deactivated by poisoning of catalytically active sites and by pore blockage due to the deposition of carbonaceous and/or metallic deposits has been studied. A simple mathematical model that has previously been successfully used by other investigators to describe phenomena of deactivation during catalytic coal liquefaction and coal-liquid hydrotreatment processes has been analyzed in detail, and it has been shown successfully that this model predicts that catalyst size, pore size, and pore size distribution have a pronounced effect on overall catalyst performance in agreement with existing experimental observations.

Admittedly, an oversimplified model in terms of the description of the reaction and diffusion processes occurring under realistic experimental conditions has been utilized here.

The main qualitative features, however, of the overall catalytic behavior predicted here are the result of basic strongly counteracting, underlying physical processes. An open catalytic pore structure facilitates diffusion of large reactant molecules, which in turn results in a more rapid catalyst deactivation and catalyst pore volume closure. As such, the types of catalytic behavior described here are not strongly dependent on the particular kinetic, diffusion, and pore

structure model employed, but are closely associated with macromolecular catalytic reacting systems that deactivate by simultaneous active site poisoning and pore blockage.

NOMENCLATURE

a	stoichiometric constant
A_0	area of pore
A_{im}	effective diffusion area of the pore
B	parameter defined in Eq. (23d)
b	coke size parameter, $V_c C_t \pi_0 / A_0$
b_1	dimensionless coke size parameter, $2V_c C_t / r_{Am}$
C_{cs}	concentration of sites covered by coke
C_i	concentration of species i in the catalyst pore
C_t	initial concentration of catalytic sites
D_{ie}	effective diffusivity of species i defined in Eq. (7a)
D_{io}	bulk diffusivity of species i
K_d	reaction constant for deactivation reaction
K_r	reaction constant for main reaction
L	half-length of pore
N	number of pores
P_1, P_2, P_3, P_4	parameters defined in Eqs. (15)–(18)
r	initial radius of pore
R_i	rate of reaction for species i
R_i^P	reaction rate for species i for the whole particle
R_i^V	reaction rate per unit volume for species i
R_i^W	reaction rate per unit weight for species i
r_{im}	effective diffusion radius for species i
S	selectivity, K_d/K_r
S_g	surface area per unit weight
S_x	geometric surface area
t	time
V_c	volume of coke molecule
V_g	void volume per unit weight
V_p	volume of catalyst particle
x	length of pore variable
X	dimensionless concentration of species A, C_A/C_{A0}
Y	dimensionless concentration of species B, C_B/C_{A0}
Z	dimensionless concentration of sites covered by coke, C_{cs}/C_t

Greek Symbols

α	fraction of sites covered by coke, uniform fouling
γ_1	$L^2 K_d C_{A0}/D_{A0}$
γ_2	D_{B0}/D_{A0}
ε	porosity of catalyst particle
ε_p	local porosity in pore
η_i	effectiveness factor for species i
θ	dimensionless time, $tK_d C_{A0}$
λ_{io}	initial pore size parameter, r_{im}/r
λ_i	pore size parameter defined in Eq. (7b)
ξ	x/L
π_o	initial perimeter of pore
ρ_p	density of catalyst particle
ρ_s	density of solid
σ	shape factor for pore size distribution, Eq. (27)
ϕ	modified Thiele modulus, $L(2K_r C_t / r_{Am} D_{A0})^{1/2}$
ϕ_I	$\phi(\lambda_{A0}/F(\lambda_{A0}))^{1/2}$
ϕ_u	$\phi[\lambda_{A0}(1-\alpha)/F(\lambda_A)\varepsilon_p]^{1/2}$

ACKNOWLEDGMENT

This work was supported in part by the U.S. Department of Energy under Contract FG22-83PCS1252.

REFERENCES

1. Maxted, E. B., *in* "Advances in Catalysis" (D. D. Eley, H. Pines, and P. B. Weisz, Eds.), Vol. 3, p. 199. Academic Press, New York, 1951.
2. Voorhies, A., *Ind. Eng. Chem.* **37**, 318 (1945).

3. Wheeler, A., *in* "Catalysis" (P. H. Emmett, Ed.), Vol. 9, p. 105. Reinhold, New York, 1955.
4. Butt, J. B., *Adv. Chem. Ser.* **109,** 259 (1972).
5. Butt, J. B., and Billimoria, R. M., ACS Symp. Ser. **72,** 288 (1978).
6. Butt, J. B., *in* "Catalyst Deactivation" (B. Delmont and G. F. Froment, Eds.), p. 21. Elsevier, Amsterdam, 1980.
7. Froment, G. F., *in* "Catalyst Deactivation" (B. Delmont and G. F. Froment, Eds.), p. 1. Elsevier, Amsterdam, 1980.
8. Hegedus, L. L., and McCabe, R. W., *in* "Catalyst Deactivation" (B. Delmont and G. F. Froment, Eds.), p. 471. Elsevier, Amsterdam, 1980.
9. Froment, G. F., *in* "Proceedings, 6th International Congress on Catalysis, London, 1976" (G. C. Bond, P. B. Wells, and F. C. Tompkins, Eds.), Vol. 1, p. 10. The Chemical Society, London, 1976.
10. Polinski, L. M., Stiegel, G. J., and Saroff, L., *Ind. Eng. Chem. Process Des. Dev.* **20** (3), 470 (1982).
11. Stiegel, G. J., Polinski, L. M., and Tischer, R. E., *Ind. Eng. Chem. Process Des. Dev.* **21**(3), 477 (1982).
12. Stiegel, G. J., Tischer, R. E., and Polinski, L. H., "Hydroprocessing of Solvent Refined Coal: Catalyst Screening Results," U.S. DOE Report No. DOE/PETC/TR-82/7(DE82008568), 1982.
13. Chiou, M. J., and Olson, J. H., *ACS Symp. Ser.* **23,** 1421 (1978).
14. Chang, H. J., Seapan, M., and Crynes, B. L., *ACS Symp. Ser.* **196,** 309 (1981).
15. Shah, Y. T., "Reaction Engineering in Direct Coal Liquefaction," Addison–Wesley, Reading, Mass., 1981.
16. Wei, J., and Wei, R. G., *Chem. Eng. Commun.* **13,** 251 (1982).
17. Androutsopoulos, G. P., and Mann, R., *Chem. Eng. Sci.* **33,** 673 (1978).
18. Beeckman, J. W., and Froment, G. F., *Chem. Eng. Sci.* **4,** 805 (1980).
19. Beeckman, J. W., and Froment, G. F., *Ind. Eng. Chem. Fundam.* **18,** 245 (1979).
20. Beeckman, J. W., and Froment, G. F., *Ind. Eng. Chem. Fundam.* **21,** 243 (1982).
21. El-Kady, F. Y. A., and Mann, R., *J. Catal.* **69,** 147 (1981).
22. Tsakalis, K. S., M.S. thesis, University of Southern California, Los Angeles, 1983.
23. Stein, T. R., Cabal, A. V., Callen, R. B., Dabkowski, J. J., Heck, R. H., Sympson, C. A., and Shih, S. S., EPRI Report No. AF-873, 1978.
24. Satterfield, C. N., Colton, C. K., and Pitcher, W. J., *AIChE J.* **19,** 628 (1973).
25. Ma, Y. H., and Gabriel, G. A., *ACS Symp. Ser.* **23,** 1437 (1978).
26. Rajagopalan, K., and Luss, D., *Ind. Eng. Chem. Process Des. Dev.* **18,** 459 (1979).
27. Masamune, S., and Smith, J. M., *AIChE J.* **12,** 384 (1966).